

# Using Random Forests to Classify $W^+W^-$ and $t\bar{t}$ Events

J. Lovelace Rainbolt<sup>1</sup>, Thoth Gunter<sup>1</sup>, and Michael Schmitt<sup>1</sup>

<sup>1</sup>Department of Physics and Astronomy, Northwestern University, Evanston, IL 60091

November 28, 2021

## 1 Introduction

The Large Hadron Collider at CERN collides proton beams at a center-of-mass energy of 7–8 TeV, and the experiments arrayed there gather immense data sets rich with information based on reconstructed particles and other objects. In this context, an “event” corresponds to a beam crossing in which one or more pairs of protons collide and produce dozens or even hundreds of particles. Physicists can identify many “features” in these events that allow them to be classified. For example, an event with a pair of oppositely-charged energetic leptons (electrons or muons), missing transverse energy, and a pair of jets could be selected as a candidate  $pp \rightarrow t\bar{t}$  event, where “ $t$ ” stands for a top quark. Event classification is essential for measuring cross sections and also in the search for new particles and phenomena.

Measurements of the cross section  $\sigma_{WW}$  for the process  $pp \rightarrow W^+W^-$  provide important tests of the standard model (SM) of particle physics. The first measurements [1, 2] focus on the case in which both  $W$  bosons decay leptonically, in which case  $W^+W^-$  events are characterized by two features shared with  $t\bar{t}$  events: two oppositely-charged energetic leptons and missing transverse energy. The number of reconstructed jets allows one to distinguish  $W^+W^-$  from  $t\bar{t}$  events on a statistical basis; the  $t\bar{t}$  “background” to the  $W^+W^-$  “signal” is nearly eliminated by rejecting events with any jets, but with a significant reduction of the signal. Currently, the measured values for  $\sigma_{WW}$  are larger than predicted by advanced theoretical calculations (see the Appendix). It has been suggested that the requirement of zero jets (known as the “jet veto”) is responsible for the discrepancy [3–5].

We have conducted an exercise in supervised machine learning, in which we use a Random Forest (RF) classifier to separate events from the two similar processes  $pp \rightarrow W^+W^-$  and  $pp \rightarrow t\bar{t}$ . RF classifiers have been used in particle physics by the DØ Collaboration [6–9] and by the BaBar Collaboration [10, 11]. Our exercise is a step toward a broader application of RF classifiers and is meant only to explore the RF classifier in a specific and well-defined case. The results are compared to a version of the original analysis published by the CMS Collaboration [1]. We find that the RF classifier provides a significantly more powerful rejection of  $t\bar{t}$  background than the standard analysis (which we will refer to as the “standard cuts” analysis), allowing a much higher  $W^+W^-$  yield for the same number of  $t\bar{t}$  events. Furthermore, the application of a cut on the output of the RF classifier hardly alters the distribution of the number of jets in  $W^+W^-$  events, in principle allowing for an incisive test of the claim that the discrepancy between the measured and the predicted values for  $\sigma_{WW}$  stems from the distribution of the number of jets.

## 2 Statement of the Problem

In the typical hadron collider analysis, the main background in the  $W^+W^-$  signal sample comes from  $t\bar{t}$  events. Our goal is to study the separation of  $W^+W^-$  and  $t\bar{t}$  events by classifying them as effectively as possible. We are interested mainly in how the RF classifier makes use of the features of the events; we are not trying to replicate a bona fide cross section measurement in a high-luminosity collider environment. For this purpose, we use the PYTHIA event generator [13]. We do not attempt to simulate the detector response. We do, however, limit the fiducial region to  $|\eta| < 2.4$  for leptons, and  $|\eta| < 4.7$  for jets. There are no inefficiencies and no contamination in the identified electron, muon, and jet collections (including  $b$ -tagging). For these reasons, the performance reported here will be unrealistic as will be reflected in the efficiencies obtained by applying the standard cuts; they are more performant than when a realistic simulation is used. Nonetheless, the relative difference between the standard cuts analysis and the RF classifier approach should be indicative.

A pre-selection of events is based on the most basic features. There must be two leptons of opposite charge, and they both must satisfy  $p_T > 20$  GeV and  $|\eta| < 2.4$ . Jets are reconstructed with the PYCLUS routine native to PYTHIA, for  $|\eta| < 4.7$  and  $p_T > 15$  GeV. Various kinematic quantities are calculated at the level of the PYTHIA event generator and are summarized in Table 1. In this context, “transverse” means transverse to the beam line, so  $p_T$  refers to the component of a momentum vector that is transverse to the beam. The azimuthal angle is denoted by  $\phi$ . The missing transverse energy,  $E_T^{\text{miss}}$ , is calculated as the vector sum of the momenta of all neutrinos in the event – detector resolution effects are not taken into account. The “projected” missing transverse energy,  $E_{T\text{proj}}^{\text{miss}}$ , takes into account the possible mismeasurement of lepton energies in Drell-Yan events and is specified in Ref. [1]. A jet that aligns with a  $b$  quark is considered a  $b$  jet with no inefficiency and no background. A kinematic quantity that is absent (for example, the  $p_{T3}^{\text{jet}}$  for an event with only two jets) is set to  $-99$ . An integer flag,  $F_{\ell\ell}$ , has value  $-2$  for an event with an  $e^+e^-$  pair,  $-1$  for a  $\mu^+\mu^-$  pair, and  $+1$  for an  $e^\pm\mu^\mp$  pair.

Table 1: Summary of kinematic quantities used as input features to the random forest

$p_{T1}$	transverse momentum of the leading lepton
$p_{T2}$	transverse momentum of the trailing lepton
$q_T$	transverse momentum of the lepton pair
$M_{\ell\ell}$	di-lepton invariant mass
$\Delta\phi$	difference in azimuthal angle between the leptons
$N_\ell^{\text{extra}}$	number of extra leptons
$p_T^{\text{extra}}$	$p_T$ of the leading extra lepton, if any
$N_{\text{jet}}$	number of hadronic jets
$p_{Ti}^{\text{jet}}$	$p_T$ of the $i^{\text{th}}$ jet
$N_{b\text{-jet}}$	number of jets with $b$ -hadrons
$E_T^{\text{miss}}$	missing transverse energy
$E_{T\text{proj}}^{\text{miss}}$	“projected” missing transverse energy
$\Delta\phi_{\ell\ell\text{miss}}$	angle between the lepton pair and the missing momentum vector
$\Delta\phi_{\ell\ell j}$	angle between the lepton pair and the leading jet
$F_{\ell\ell}$	flag to indicate lepton channel

In order to compare to a standard analysis, such as the one developed by the CMS Collaboration [1],

Table 2: Selection criteria for the cut-based analysis

$M_{\ell\ell} > 12 \text{ GeV}$ $q_T < 45 \text{ GeV}$ $\Delta\phi_{\ell\ell j} < 2.8798 \text{ rad}$ $N_{\ell}^{\text{extra}} = 0$ $N_{\text{jet}} = 0$ $N_{b\text{-jet}} = 0$ If $F_{\ell\ell} < 0$ then $M_{\ell\ell} < 76 \text{ GeV}$ or $M_{\ell\ell} > 106 \text{ GeV}$ If $F_{\ell\ell} < 0$ then $E_{T\text{proj}}^{\text{miss}} < 20 \text{ GeV}$ , or if $F_{\ell\ell} = 1$ then $E_{T\text{proj}}^{\text{miss}} < 45 \text{ GeV}$
--

we tried to implement a cut-based selection of  $W^+W^-$  events. The cuts are specified in Table 2 and are applied to events that pass the pre-selection.

### 3 Method

For this study, we employed the freeware package OPENCV [12], written in C++ with no reference to external libraries or packages. We found this package to be fast, effective, and easy to use.

The PYTHIA event generator was run to generate a fixed number of events from a given process passing the preselection. For each event, the kinematic quantities listed in Table 1 were written to a formatted file and labeled according to the physics process that was simulated:  $K = 1$  for  $pp \rightarrow W^+W^-$ ,  $K = 2$  for  $pp \rightarrow t\bar{t}$ , and  $K = 3$  for the Drell-Yan production of lepton pairs. Independent training and testing sets were generated, each consisting of  $10^4$   $W^+W^-$  events,  $10^4$   $t\bar{t}$  events, and 4998 Drell-Yan events. Since the number of  $W^+W^-$  and  $t\bar{t}$  events is the same, the RF responds only to the features and not to the frequency of events. The Drell-Yan events are easily eliminated so we do not consider them further, in this study.

The RF was specified to have a population of 1000 trees. Since the RF does not overfit, its performance improves as the number of trees increases. However, growing the forest is a computationally expensive process whose cost increases with the number of trees, and whose benefit becomes negligible once this number is sufficiently high (over several hundred). A greater number of trees is also beneficial in that it allows for more precision in the output of the classifier,  $Y$ , which is given by the number of trees categorizing an event as signal divided by the total number of trees. It is therefore quantized at the level of  $\Delta Y = 0.001$  in our case.

Each tree was set to have a maximum depth of 15 nodes, with the number of active features at each node set to the square root of the total number of features. The tree depth is the number of node splits through which a case is processed before the tree assigns it a final classification. A greater depth results in each tree eliminating a smaller number of the training cases at each node, making for a more refined analysis. The tree determines where to split each node from a subset of features, known as the active features, which is selected randomly at each node. The feature supplying the best possible division at each node is the one used to make the split, and choosing that feature from a randomly-selected subset reduces the correlation among trees. In most cases, a subset size near the square root of the total number of features provides the most accurate performance of the RF. Nonetheless, we tried wide variations of this parameter and the others, and found that they were

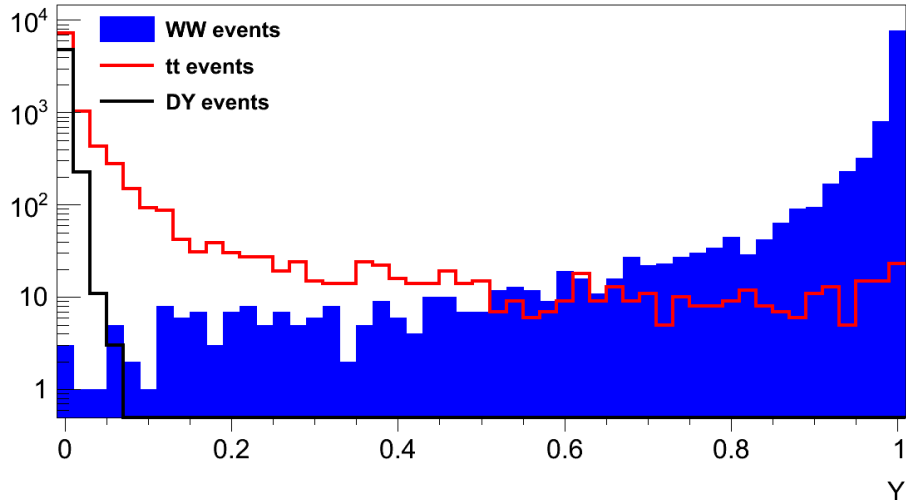


Figure 1: Histogram of the output variable  $Y$  from the random forest. The blue histogram is  $W^+W^-$  signal and the red histogram is the  $t\bar{t}$  background. The blue line represents the Drell-Yan background. A cut  $Y > Y_{\text{cut}}$  selects a relatively pure signal sample.

not critical provided they were not too small.

The RF was trained to give an output of  $Y = 1$  for signal  $W^+W^-$  events and  $Y = 0$  for background  $t\bar{t}$  and Drell-Yan events. After training (which takes only about a minute), we presented the RF with the test set and made a histogram of the output  $Y$  – see Fig. 1. The effective separation of  $W^+W^-$  signal events from  $t\bar{t}$  and Drell-Yan background events is evident.

## 4 Results

A requirement  $Y > Y_{\text{cut}}$  amounts to a selection of signal  $W^+W^-$  events and a rejection of  $t\bar{t}$  and Drell-Yan events. If we vary  $Y_{\text{cut}}$  from low to high values, we can trace out a receiver operator characteristic (ROC) curve. Following tradition in particle physics, we use the efficiency for  $W^+W^-$  events,  $\epsilon_{WW}$ , and the efficiency for  $t\bar{t}$  events,  $\epsilon_{tt}$ , to specify the curve. They are determined using the test set of events; recall that these events have passed the preselection so  $\epsilon_{WW} \rightarrow 1$  means that all events with a pair of oppositely-charged leptons with  $p_T > 20$  GeV and  $|\eta| < 2.4$  are selected.

Figure 2 shows the ROC curve for the RF. The jumps and non-smooth behavior at low values of  $\epsilon_{tt}$  are consequences of the discretization of  $Y$ , not of the size of the testing sample. The fact that the curve bends sharply toward the lower-right corner of the plane, where  $\epsilon_{WW}$  is high and  $\epsilon_{tt}$  is low, reflects the excellent separation of signal and background events. The performance of the standard cuts analysis is represented by the red dot. Clearly, it is less performant than the RF. For a given  $t\bar{t}$  efficiency, the RF achieves a higher signal efficiency, and likewise, for a given  $W^+W^-$  efficiency, it achieves a greater background rejection. The Drell-Yan background is easily eliminated as is also the case for the standard cuts analysis: in a realistic analysis, the Drell-Yan background appears

through reconstruction and detector effects, which are outside the scope of this study. Note that in the CMS analysis [1], the primary background is, by far,  $t\bar{t}$ .

We point out that the efficiencies we obtain for the standard cut are significantly higher than in the actual CMS analysis because our simulation is idealized. Presumably, the efficiencies we obtain for the RF are also “optimistic” and would not be achieved by a RF trained and evaluated with a realistic simulation. Nonetheless, the difference in the performance of the RF and the standard cuts analysis seen should still carry over to an analysis with a realistic simulation of the detector response.

Several quantities are available to the RF that were not used by the standard cuts analysis. One might suspect that the improved performance resulted from the availability of more information. We trained a second RF in which we restricted the kinematic quantities to those listed in Table 2. The performance is only slightly weaker than the original RF, indicating that the RF technique, and not the additional kinematic quantities, brings the better performance.

The goal of the LHC analyses is to measure the cross section  $\sigma_{WW}$ . In order to gauge the impact of the RF on this goal, we define a figure of merit that captures the statistical power of a data set. In the context of this study, the cross section can be defined:

$$\sigma_{WW} = \frac{N_{WW} - N_{t\bar{t}}}{A_{WW}\epsilon_{WW}\mathcal{L}} \quad (1)$$

where  $A_{WW}$  is the acceptance (*i.e.*, the fraction of  $W^+W^-$  events passing the preselection),  $\mathcal{L}$  is the integrated luminosity,  $N_{WW}(= A_{WW}\epsilon_{WW}\mathcal{L}\sigma_{WW})$  is the number of selected  $W^+W^-$  signal events, and  $N_{t\bar{t}}(= A_{t\bar{t}}\epsilon_{t\bar{t}}\mathcal{L}\sigma_{t\bar{t}})$  is the number of selected  $t\bar{t}$  background events. Since  $A_{t\bar{t}} \approx A_{WW}$ , the point of the analysis is to work in a regime in which  $\epsilon_{WW} \gg \epsilon_{t\bar{t}}$ .

We take  $A$ ,  $\epsilon$ , and  $\mathcal{L}$  to be sufficiently well known, and focus on the stochastic quantities  $N_{WW}$  and  $N_{t\bar{t}}$ . Our figure of merit is the relative statistical uncertainty on  $\sigma_{WW}$ :

$$F = \frac{\sqrt{N_{WW} + N_{t\bar{t}}}}{N_{WW} - N_{t\bar{t}}} = \frac{\sqrt{A_{WW}\epsilon_{WW}\sigma_{WW} + A_{t\bar{t}}\epsilon_{t\bar{t}}\sigma_{t\bar{t}}}}{A_{WW}\epsilon_{WW}\sigma_{WW} - A_{t\bar{t}}\epsilon_{t\bar{t}}\sigma_{t\bar{t}}}. \quad (2)$$

We calculate that  $A_{WW} = 0.762 A_{t\bar{t}}$  based on simulations. The numerical values of the cross sections at 8 TeV are  $\sigma_{WW} = 57$  pb [14] and  $\sigma_{t\bar{t}} = 246$  pb [15]. Table 3 compares values of  $F$  for the standard cuts analysis and three operating points for the RF analysis. The numerical values indicate that the RF analysis could lead to a statistically more precise measurement than the standard cuts analysis. For example, setting  $Y_{\text{cut}}$  so that  $\epsilon_{t\bar{t}}$  is the same as in the standard cuts analysis, the signal efficiency is three times higher and the corresponding statistical uncertainty would be nearly half as small. This operating point is near the optimal point defined by the lowest value of  $F$ . Figure 3 shows the variation of  $F$  with  $Y_{\text{cut}}$ ; a shallow minimum is observed near 0.1 reflecting the strong separation illustrated in Fig. 1. If, instead of aiming for the best statistical precision, we aim for the same statistical uncertainty as the standard cuts analysis, then the signal efficiency is essentially unity.

The crucial piece of the standard cuts analysis is the so-called “jet veto.” As mentioned earlier, it has been suggested that the Monte Carlo event simulators in use by the LHC collaborations are not sufficiently accurate, and that the discrepancy between the measured values of  $\sigma_{WW}$  and the predicted value is caused by an incorrect value of  $\epsilon_{WW}$  stemming from the jet veto.

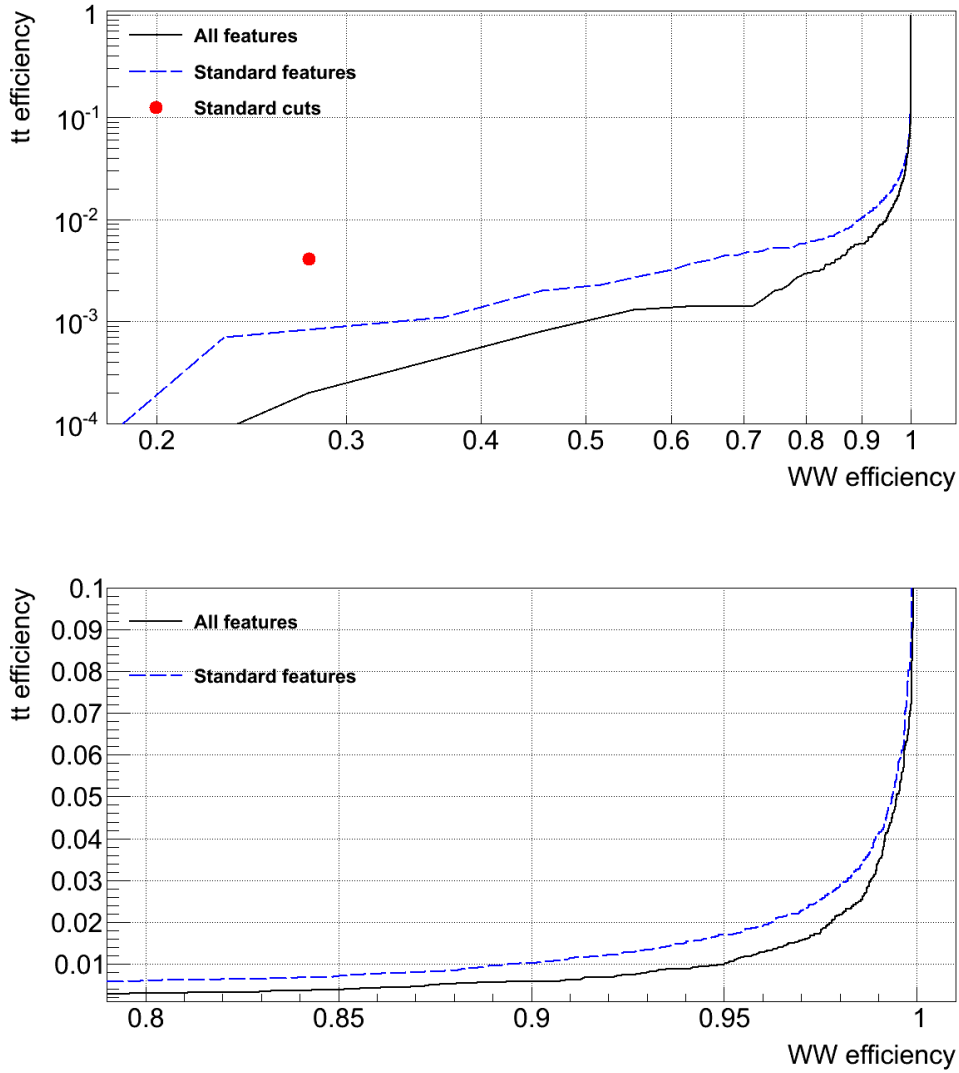


Figure 2: Receiver operator curves expressed as in terms of the selection efficiency for signal  $W^+W^-$  events and background  $t\bar{t}$  events. The selection efficiency is defined with respect to events passing the fiducial requirements. The solid black line is the result obtained with all features listed in Table 1 while the dashed blue line is the result obtained only with the features used in the standard cuts analysis (Table 2). The performance of the standard cuts is indicated by the red dot in the upper plot. The lower plot shows a zoom of the high- $\epsilon_{WW}$  region.

Table 3: Comparison of the figure of merit ( $F$ ) for the standard cuts analysis and three RF operating points

analysis	$Y_{\text{cut}}$	$\epsilon_{WW}$	$\epsilon_{tt}$	$F$
standard cuts	-	0.2767	0.0041	0.417
RF low- $\epsilon_{tt}$	0.965	0.8576	0.0041	0.217
RF best- $F$	0.914	0.9061	0.0058	0.214
RF high- $\epsilon_{WW}$	0.072	0.9987	0.0772	0.419

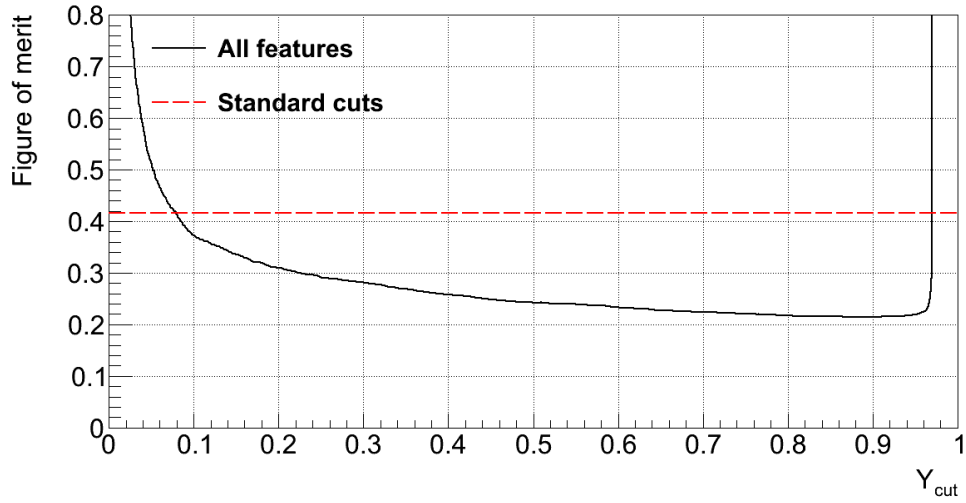


Figure 3: Figure of merit as a function of the cut on the RF output variable,  $Y_{\text{cut}}$ .

An intriguing feature of the RF selection is that it does not result in strong cuts in any variable. Some trees may make use of a given variable while others will not; the result is a softer impact on the original distribution of that variable.

We studied the  $N_{\text{jet}}$  distribution before and after applying a selection cut on the RF output. Remarkably, there was *no impact on  $N_{\text{jet}}$  at all* if the cut was not too strong. For example, if we chose to match the value of  $\epsilon_{tt}$  obtained with the standard cuts analysis, then with the RF the value of  $\epsilon_{WW}$  is very high and the  $N_{\text{jet}}$  distribution is unchanged, as illustrated in Fig. 4. This feature of the RF would allow, in principle, a direct check of the  $N_{\text{jet}}$  distribution in  $pp \rightarrow W^+W^-$  events, and innocuate the cross section measurement from any systematic bias coming from the jet veto. In a more general sense, the fact that the RF classifier induces relatively gentle distortions of the distributions of key kinematic quantities (certainly less abrupt than applying a cut) suggests that systematic uncertainties due to the modeling of these distributions should be significantly reduced or perhaps effectively eliminated.

A common concern with multi-variate methods is the potential sensitivity to the training set. In a real analysis, one would use simulated events to train the RF, and then apply the RF to real events recorded with the detector. If the fidelity of the simulation is imperfect, then a bias may result that is difficult to quantify. Since we do not simulate the detector at all, we cannot address this question carefully. Nonetheless, we did apply a gross distortion to the  $E_T^{\text{miss}}$ , rescaling it upward by 10% in the test sample (but not in the training sample). The change in the efficiencies are  $\Delta\epsilon_{WW} = -0.05$  and  $\Delta\epsilon_{tt} = 0.002$ ; the figure of merit changed by only  $\Delta F = 0.006$ .

Finally, we checked one of the main virtues of the RF classifier: it should be able to classify an event even if it is missing one or more features. For example, one might disregard the  $E_T^{\text{miss}}$  for an event (and of course the associated variables) if there was evidence for anomalous noise in the calorimetry. For a standard analysis, the event must be discarded; one usually restricts the analysis only to those data sets for which the entire detector was operating well. If “bad” or otherwise faulty data could be recovered using an RF, then a significant gain in the size of the data set could be realized. We made a test in which we masked the  $E_T^{\text{miss}}$  for a random sample of 10% of the testing set (but not in the training set). Remarkably, the loss in  $\epsilon_{WW}$  was only 2.4%.

## 5 Conclusions

We have carried out an exercise in the application of random forest classifiers to separating signal and background events in particle physics. A technically similar exercise was performed by members of the MAGIC Collaboration, who were separating photon- and hadron-initiated atmospheric showers [16]. Other applications of random forests in high-energy physics are documented in [6–11].

For this exercise, we produced training and testing samples at the parton level, and presented them to a random forest. The RF performance surpasses the performance of a standard cut-based analysis. Furthermore, the distortion of the distributions of key kinematic event features is relatively slight, suggesting that systematic uncertainties due to modeling might be reduced. Finally, the RF we developed can tolerate missing features such as the missing transverse energy without a severe degradation of its performance, a characteristic that may allow less than perfect data to be utilized in measurements and searches for new particle and phenomena.



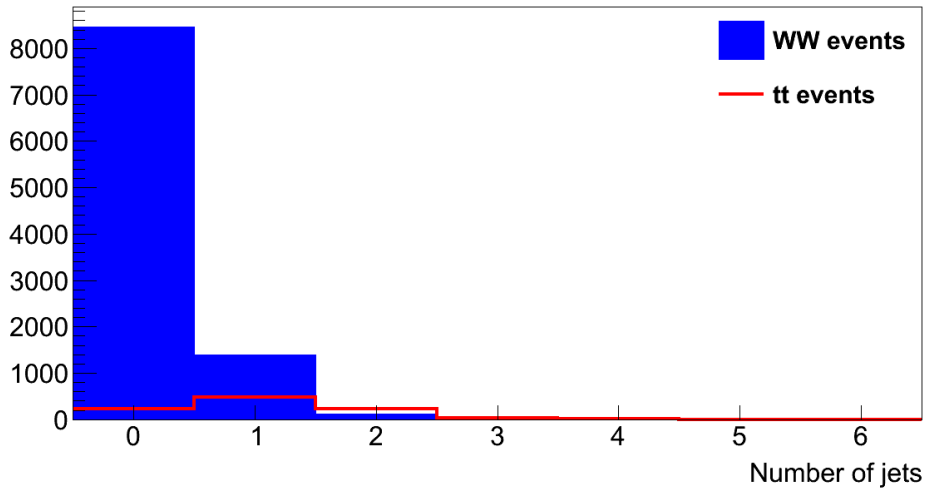
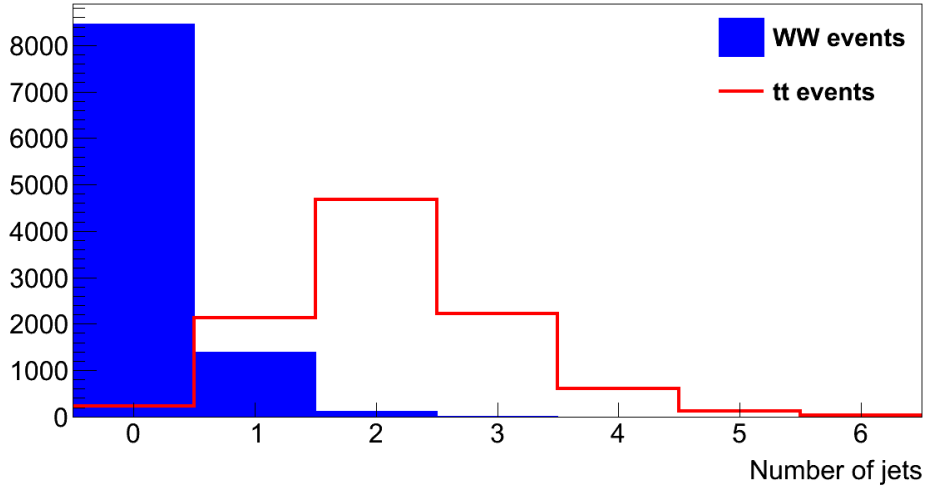


Figure 4: Distribution of the number of jets,  $N_{\text{jet}}$ . The solid blue histogram represents the  $W^+W^-$  distribution, and the thick red line represents the  $t\bar{t}$  distribution. The top plot shows the distributions after the pre-selection (there are  $10^4$  entries for each), and the bottom plot shows the distributions for the high- $\epsilon_{WW}$  working point listed in Table 3. The  $W^+W^-$  distribution is essentially unchanged despite the strong suppression of  $t\bar{t}$  events by a factor of nine.

## Appendix: $\sigma_{WW}$ Measurements

The measured cross sections for  $pp \rightarrow W^+W^-$  are higher than predicted at the level of two or more standard deviations. Table 4 gives a summary. The CMS and ATLAS collaborations have made two measurements each: one at  $\sqrt{s} = 7$  TeV and the other at 8 TeV. The CMS and ATLAS values are mutually consistent, and are higher than the theoretical predictions. For the calculations of the ratios listed in the table, the asymmetric uncertainties have been symmetrized.

Table 4: Summary of measurements of  $\sigma_{WW}$  in pb. For the measured values, the first uncertainty is statistical, the second is systematic, and the third comes from the luminosity. The last column shows the ratio of the experimental value and the theoretical one.

Collaboration	$\sqrt{s}$ (TeV)	measured	theoretical	ratio
ATLAS [2] (prelim.)	8	$71.4 \pm 1.2^{+5.0}_{-4.4} +2.2_{-2.1}$	$58.7^{+3.0}_{-2.7}$	$1.22 \pm 0.11$
CMS [1]	8	$69.9 \pm 2.8 \pm 5.6 \pm 3.1$	$57.3^{+2.3}_{-1.6}$	$1.22 \pm 0.13$
ATLAS [17]	7	$51.9 \pm 2.0 \pm 3.9 \pm 2.0$	$44.7^{+2.1}_{-1.9}$	$1.16 \pm 0.12$
CMS [18]	7	$52.4 \pm 2.0 \pm 4.5 \pm 1.2$	$47.0 \pm 2.0$	$1.12 \pm 0.12$

## References

- [1] CMS Collaboration, “Measurement of  $W^+W^-$  and  $ZZ$  production cross sections in pp collisions at  $\sqrt{s} = 8$  TeV,” Phys. Lett. B **721**, 190 (2013) [arXiv:1301.4698 [hep-ex]].
- [2] ATLAS Collaboration, “Measurement of the  $W^+W^-$  production cross section in proton-proton collisions at  $\sqrt{s} = 8$  TeV with the ATLAS detector,” conference note ATLAS-CONF-2014-033
- [3] P. Meade, H. Ramani and M. Zeng, “Transverse momentum resummation effects in  $W^+W^-$  measurements,” arXiv:1407.4481 [hep-ph].
- [4] P. Jaiswal and T. Okui, “An Explanation of the  $WW$  Excess at the LHC by Jet-Veto Resummation,” arXiv:1407.4537 [hep-ph].
- [5] P. F. Monni and G. Zanderighi, “On the excess in the inclusive  $W^+W^- \rightarrow l^+l^-\nu\bar{\nu}$  cross section,” arXiv:1410.4745 [hep-ph].
- [6] V. M. Abazov *et al.* [D0 Collaboration], “Measurement of the top quark pair production cross section in the lepton+jets channel in proton-antiproton collisions at  $\sqrt{s}=1.96$  TeV,” Phys. Rev. D **84**, 012008 (2011) [arXiv:1101.0124 [hep-ex]].
- [7] V. M. Abazov *et al.* [D0 Collaboration], “Measurements of  $WW$  and  $WZ$  production in  $W$  + jets final states in  $p\bar{p}$  collisions,” Phys. Rev. Lett. **108**, 181803 (2012) [arXiv:1112.0536 [hep-ex]].
- [8] V. M. Abazov *et al.* [D0 Collaboration], “Combined search for the Higgs boson with the D0 experiment,” Phys. Rev. D **88**, no. 5, 052011 (2013) [arXiv:1303.0823 [hep-ex]].
- [9] V. M. Abazov *et al.* [D0 Collaboration], “Improved  $b$  quark jet identification at the D0 experiment,” Nucl. Instrum. Meth. A **763**, 290 (2014) [arXiv:1312.7623 [hep-ex]].

- [10] J. P. Lees *et al.* [BaBar Collaboration], “Exclusive Measurements of  $b \rightarrow s\gamma$  Transition Rate and Photon Energy Spectrum,” *Phys. Rev. D* **86**, 052012 (2012) [arXiv:1207.2520 [hep-ex]].
- [11] J. P. Lees *et al.* [BaBar Collaboration], “Search for di-muon decays of a low-mass Higgs boson in radiative decays of the  $\Upsilon(1S)$ ,” *Phys. Rev. D* **87**, no. 3, 031102 (2013) [arXiv:1210.0287 [hep-ex]].
- [12] OPENCV version 2.4.9, downloaded from [opencv.org](http://opencv.org)
- [13] T. Sjostrand, S. Mrenna and P. Z. Skands, “PYTHIA 6.4 Physics and Manual,” *JHEP* **0605**, 026 (2006) [hep-ph/0603175].
- [14] This value was obtained using MCFM.
- [15] M. Czakon, P. Fiedler and A. Mitov, “Total Top-Quark Pair-Production Cross Section at Hadron Colliders Through  $O(\alpha_s^4)$ ,” *Phys. Rev. Lett.* **110**, no. 25, 252004 (2013) [arXiv:1303.6254 [hep-ph]].
- [16] R. K. Bock, A. Chilingarian, M. Gaug, F. Hakl, T. Hengstebeck, M. Jirina, J. Klaschka and E. Kotrc, “Methods for multidimensional event classification: A case study using images from a Cherenkov gamma-ray telescope,” *Nucl. Instrum. Meth. A* **516**, 511 (2004).
- [17] ATLAS Collaboration, “Measurement of  $W^+W^-$  production in pp collisions at  $\sqrt{s} = 7$  TeV with the ATLAS detector and limits on anomalous  $WWZ$  and  $WW\gamma$  couplings,” *Phys. Rev. D* **87** 112001 (2013) [Erratum-ibid. **D88** 079906 (2013)] [arXiv:1210.2979 [hep-ex]].
- [18] CMS Collaboration, “Measurement of the  $W^+W^-$  Cross section in  $pp$  Collisions at  $\sqrt{s} = 7$  TeV and Limits on Anomalous  $WW\gamma$  and  $WWZ$  couplings,” *Eur. Phys. J. C* **73**, 2610 (2013) [arXiv:1306.1126 [hep-ex]].